Available online at www.sciencedirect.com
ScienceDirect
Journal of Sound and Vibration 312 (2008) 584–605
JOURNAL OF SOUND AND VIBRATION
www.elsevier.com/locate/jsvi

On the principle of impulse damper: A concept derived from impact damper

S. Chatterjee

Department of Mechanical Engineering, Bengal Engineering and Science University, Shibpur, Howrah 711 103, West Bengal, India

Received 10 November 2006; received in revised form 14 June 2007; accepted 2 November 2007
Available online 20 February 2008

Abstract

The present article discusses a new principle of active vibration control of lightly damped flexible structural members. The basic scheme mimics the working principle of impact dampers. Control efforts are in the form of impulses generated by expanding and contracting a mass loaded lead zirconium titanate (PZT) stack actuator at suitable values of the states of the system. Efficacy of the damper is demonstrated in mitigating free vibration, forced vibration and self-excited vibration of a single-degree-of-freedom primary system. Effects of various parameters are studied to reveal the existence of optimum control parameters in controlling free vibration. Finally, a dynamic control law is proposed to generate the hysteretic control commands for expanding and contracting the actuator. The hysteretic part of the control command is generated by a first-order nonlinear ordinary differential equation (ODE). The proposed scheme is thought to be useful for controlling vibrations of a wide class of systems ranging from macro- to microscale applications like microelectromechanical systems (MEMS), microrobots, and other micromachines, etc. If adaptively used, the damper can perform optimally without requiring an explicit mathematical model of the system and the global dynamic information thereof.

1. Introduction

Controlling unwanted vibrations of mechanical and structural components is always a significant research area for engineers and scientists. Various active and passive devices have been theoretically studied and implemented in practice. These devices include dynamic vibration neutralizers, pendulum absorbers, autoparametric vibration absorbers, impact dampers, etc. Each of these devices has its relative merits and demerits.

The major motivation of the present work comes from the principle of impact damper. Impact damper finds prominent mentions in the literature mainly because of its simple constructional features and rich dynamic characteristics. An impact damper consists of a loose or elastically suspended mass inside a properly designed cavity in the primary vibrating body. A large number of research works have been reported on the design and performance of impact dampers for controlling free and forced vibration of linear and nonlinear systems. Only a few of the recent works along with some classic papers on impact dampers are cited here [1–21]. The most effective dynamic mode of operation of an impact damper in controlling resonant vibration is the symmetric,

E-mail address: shy@mech.becs.ac.in

0022-460X/$ - see front matter © 2007 Elsevier Ltd. All rights reserved.
doi:10.1016/j.jsv.2007.11.002

two impacts per cycle motion. In this mode of motion, the secondary mass undergoes repeated collisions with the primary mass each time the primary mass crosses its zero position (the static equilibrium configuration) with the secondary mass moving in the direction opposite to the primary mass. As a result, impacts are produced in the direction opposite to the velocity of the primary system. Depending upon the major source of vibrational energy, attenuation is caused either by momentum transfer (between the primary and secondary masses) or by energy dissipation during impacts.

Despite several advantages, such as simple constructional features, the use of passive impact damper is limited due to its ineffectiveness in case of broadband excitations. This is because the motion with symmetric two impacts per cycle is destabilized and thus, the impacts are not produced in the desired optimal fashion. Moreover, the optimal design of a passive impact damper is highly sensitive to the model of the primary system. Semi-active impact damper with on-line control algorithm has been proposed [22] to overcome these limitations. The procedure uses a tunable impact damper with adjustable motion-limiting stops. The secondary mass is made to undergo collisions against the stopper wall by adjusting its location at each zero-crossing of the displacement of the primary mass, with the secondary mass moving in the direction opposite to the primary mass.

Instead of using physical impacts, as in impact dampers, actively generated pulses can also be utilized for controlling structural vibrations. Several open-loop vibration control methods using active pulses have been developed [23–26] where pulses are generated to offset the response of the primary system when a suitable response variable reaches a predefined threshold value.

The present article introduces a novel method of controlling vibration of lightly damped structural members. The method is active in nature and mimics the basic principle of an impact damper. In impact dampers, vibration is mitigated by a series of impact forces generated due to the repeated collisions of an auxiliary mass with the primary system. However, the proposed scheme, instead of relying on physical impacts, generates actively controlled impulses. As the basic controlling force is impulsive in nature, the proposed damper may be rightly called as the 'impulse damper'. Keeping in view the applicability of the present method in a large class of systems ranging from macro- to microscales, a lead zirconium titanate (PZT) stack actuator is considered for generating actively controlled impulsive forces. PZT actuator offers the unique advantage of compactness of its design. However, other actuators like, MR/ER, magnetostictive, and electromagnetic actuators, etc. are equally possible alternatives as permitted by the length scale of a particular application.

2. Basic principle and mathematical model

The simplest configuration of the proposed system, considered herein, consists of a secondary mass attached to the primary vibrating body with a PZT stack actuator. When the primary mass is displaced from its neutral configuration with a positive velocity, the piezoelectric actuator expands suddenly. Because of this expansion, the secondary mass exerts an inertial reaction impulse on the primary system in the direction opposite to the movement of the primary mass. Similarly, when the primary mass is displaced from the equilibrium with a negative velocity, an opposite reactive impulse force is generated due to a sudden contraction of the PZT actuator.

Mathematical model of the proposed impulse damper is depicted in Fig. 1. The primary system is modelled as a single-degree-of-freedom spring–mass–damper (M, K, C) system. The damper mass m is attached to the primary mass by a PZT stack actuator.

2.1. Mechanical model of the PZT actuator

According to Ref. [27], the mechanical behaviour of the PZT stack can be mathematically described by the following transfer function:

$$P(s) = \frac{X_P(s)}{F_p(s) - F_e(s)} = \frac{N_p(s)}{D_p(s)}. \tag{1}$$

The above equation describes the input–output relationship between the elongation $X_p(s)$ of the actuator and the mechanical load (that drives the actuator) $F_p(s)-F_e(s)$ in the Laplace domain. Here, F_p represents the

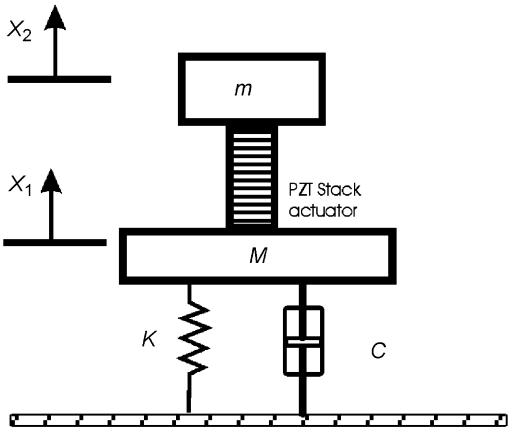

Fig. 1. Mathematical model of the proposed impulse damper.

electrically transduced force of the actuator (same as the blocking fore, i.e., the actuator force at the zero elongation condition of the actuator) and F_e is the external load acting on the actuator. $N_p(s)$ and $D_p(s)$ are the polynomials of the Laplace variable that determine the zeros and poles of the transfer function $P(s)$, respectively. Zeros and poles of the transfer characteristics of the PZT stack can be obtained from the eigenmodes of the system as described below.

The dynamics of free vibration of a PZT stack actuator of length L is described by the following PDE [27]:

$$K_p L\frac{\partial^2 w}{\partial y^2}+C_p L\frac{\partial^3 w}{\partial y^2\,\partial t}=\frac{M_p}{L}\frac{\partial^2 w}{\partial t^2}, \tag{2a}$$

where $w(y, t)$ denotes the instantaneous axial displacement of the PZT stack at an arbitrary axial location y. K_p, C_p, and M_p are the axial static stiffness, viscous damping coefficient and the mass of the stack, respectively.

Using the principle of separation of variables, the free response of the stack can be written in the following form:

$$w(y,t)=\sum_{i=1}^{\infty} Y_i(y)T_i(t). \tag{2b}$$

Substituting Eq. (2) into Eq. (1), one finally obtains the following two ordinary differential equations (ODEs):

$$Y_i''+\Omega_i^2 Y_i=0, \tag{3}$$

$$\ddot{T}_i+\Omega_i^2 L^2\frac{C_p}{M_p}\dot{T}_i+\Omega_i^2 L^2\frac{K_p}{M_p}T_i=0, \tag{4}$$

where 'dash' and 'dot' denote derivatives with respect to y and t, respectively. Ω_i is a constant, which can be obtained as described below.

The general solution of Eq. (3) is given by

$$Y_i(y)=A_i\cos(\Omega_i y)+B_i\sin(\Omega_i y). \tag{5}$$

The constants A_i and B_i can be determined from the boundary conditions. Free–free boundary conditions are appropriate for the present problem. These boundary conditions are obtained by equating the normal force at the two ends of the stack to zero, i.e.,

$$LK_p Y_i'(0)T_i(t)+LC_p Y_i'(0)\dot{T}_i(t)=0, \tag{6}$$

$$LK_p Y_i'(L)T_i(t)+LC_p Y_i'(L)\dot{T}_i(t)=0. \tag{7}$$

From Eqs. (6) and (7), one obtains the eigenmodes of the stack as

$$Y_i(y) = A_i \cos\left(\frac{i\pi y}{L}\right), \quad i = 1, 2, \ldots, \infty. \tag{8}$$

The condition corresponding to $i = 0$ is excluded because this signifies the rigid-body translation of the stack. Elongation of the stack for the ith mode is obtained as

$$\Delta L_i = Y_i(L) - Y_i(0), \tag{9}$$

where $Y_i(L)$ and $Y_i(0)$ are the modal displacements of the stack at the primary-mass side and the secondary-mass side of the actuator, respectively. It may be noted that the modal elongations of the stack are zero for the even modes. Therefore, even modes provide the zeros and odd modes provide the poles of the transfer characteristics $P(s)$. Thus, from Eq. (4) one writes

$$N_p(s) = \prod_{i=1}^{\infty} \frac{M_p}{\Omega_{2i}^2 L^2} s^2 + C_p s + K_p, \tag{10}$$

$$D_p(s) = \prod_{i=1}^{\infty} \frac{M_p}{\Omega_{2i-1}^2 L^2} s^2 + C_p s + K_p, \tag{11}$$

where $\Omega_i^2 L^2 = (i\pi/L)^2$ for $i = 1, 2, \ldots, \infty$.

For the configuration of the system considered here,

$$D_1(s) X_1(s) = -F_e(s), \tag{12}$$

$$D_2(s) X_2(s) = F_e(s), \tag{13}$$

where $D_1(s) = Ms^2 + Cs + K$ and $D_2(s) = ms^2$.

From Eqs. (1), (12), and (13), the mechanical model of the PZT stack is obtained as

$$\frac{X_p(s)}{F_p(s)} = \frac{N_p(D_1 + D_2)}{(D_1 + D_2)D_p + D_1 D_2 N_p}. \tag{14}$$

It may be noted that the blocking force $F_p(s)$ of the actuator is directly proportional to the voltage applied across the actuator. Therefore, Eq. (14) (multiplied by some constant) also represents the electromechanical characteristics of the PZT stack.

Transfer characteristics of the full system shown in Fig. 1, with the displacement of the primary mass as the output and the blocking force of the actuator as the input, is described by

$$\frac{X_1(s)}{F_p(s)} = \frac{N_p D_2}{(D_1 + D_2)D_p + D_1 D_2 N_p}. \tag{15}$$

Typical frequency response plots of the system for some realistic parameter values [27] are shown in Fig. 2. It is observed from these plots that the higher modes of the PZT stack are heavily suppressed even for small values of damping. Further suppression of the higher modes is possible by increasing the absorber mass m. Thus, a single mode model of the absorber suffices to serve the purpose of analysing the efficacy of the proposed damper.

2.2. Simplified mathematical model of the proposed system

In the foregoing, it is established that the PZT stack can be amply represented by a single mode model for some realistic parameter values. Thus, the simplified mathematical model of the system reads as

$$MX_1'' + CX_1' + KX_1 = C_p X_p' - F_a, \tag{16}$$

$$m_a X_2'' = -C_p X_p' + F_a, \tag{17}$$

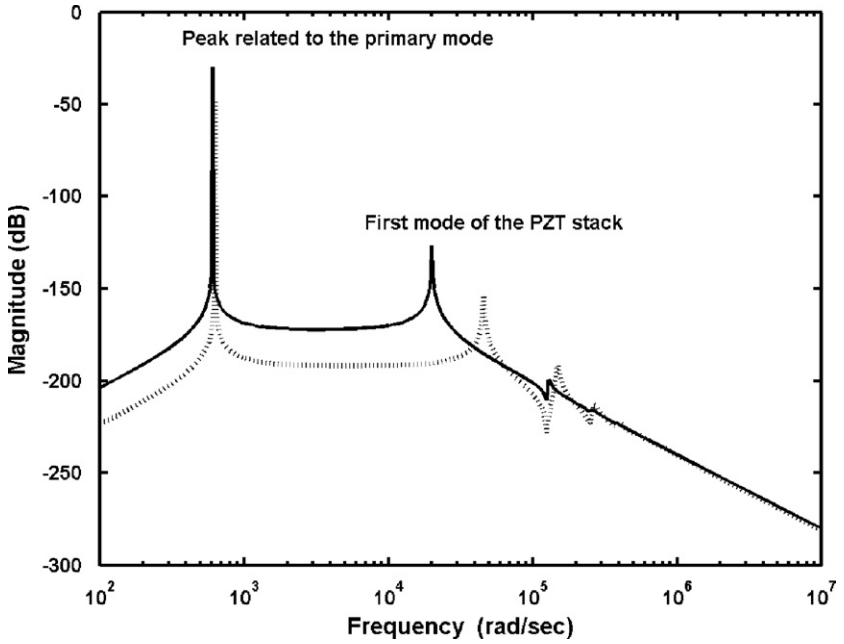

Fig. 2. Bode plot of the system characteristic given in Eq. (15). $C_p = 10\,\text{kg/s}$, $M_p = 0.1\,\text{kg}$, $C = 0$, $M = 1.0\,\text{kg}$, $K_p = 4 \times 10^7\,\text{N/m}$, and $K = 4 \times 10^5\,\text{N/m}$. ———, $m = 0.1$; ·····, $m = 0.01$.

where $X_p = X_2 - X_1$ is the elongation, F_a is the force produced by the actuator and $m_a = (M_p/\pi^2) + m$ is the effective absorber mass. Prime ($'$) denotes differentiation with respect to time t. Eq. (17) is rewritten as

$$m_a X_p'' + C_p X_p' = -m_a X_1'' + F_a. \tag{18}$$

The electromechanical characteristics of the PZT actuator is given by the following equation:

$$\begin{Bmatrix} Q_p \\ X_p \end{Bmatrix} = \begin{bmatrix} C_{\text{PZT}} & -nd_{33} \\ nd_{33} & -\frac{1}{K_p} \end{bmatrix} \begin{Bmatrix} V_p \\ F_a \end{Bmatrix}, \tag{19}$$

where Q_p, X_p, V_p, F_a represent charge, elongation, voltage, and force in the PZT actuator, respectively. C_{PZT} is the effective capacitance of the PZT actuator, d_{33} is the piezoelectric constant of each wafer, and n is the total number of wafers in the actuator. K_p^{-1} is the compliance of the actuator in short circuit condition and is given by $K_p = EA/L$, where E is the elastic modulus, A is the cross-sectional area, and L is the length of the actuator.

From Eq. (19), the following expression for the actuator force is obtained:

$$F_a = nd_{33}K_pV_p - K_pX_p. \tag{20}$$

Eqs. (16), (18), and (20) are normalized and rewritten as

$$\begin{bmatrix} 1 & 0 \\ r_m & r_m \end{bmatrix} \begin{Bmatrix} \ddot{X} \\ \ddot{Z} \end{Bmatrix} + \begin{bmatrix} 2\xi & -h_p \\ 0 & h_p \end{bmatrix} \begin{Bmatrix} \dot{X} \\ \dot{Z} \end{Bmatrix} + \begin{bmatrix} 1 & -\alpha \\ 0 & \alpha \end{bmatrix} \begin{Bmatrix} X \\ Z \end{Bmatrix} = \frac{\lambda^2}{1-\lambda^2}\alpha V \begin{Bmatrix} -1 \\ +1 \end{Bmatrix}, \tag{21}$$

where

$$X = \frac{X_1}{x_0}, \quad Z = \frac{X_p}{x_0}, \quad \omega_n = \sqrt{\frac{K}{M}}, \quad \xi = \frac{C}{2\sqrt{KM}}, \quad r_m = \frac{m_a}{M}, h_p = \frac{C_p}{M\omega_n}, \quad V = \frac{V_p}{V_{\text{ref}}}, \quad V_{\text{ref}} = \frac{\lambda^2 x_0}{(1-\lambda^2)nd_{33}},$$

$$\alpha = \frac{K_p}{K} \quad \text{and} \quad \lambda^2 = \frac{n^2 d_{33}^2 K_p}{C_{\text{PZT}}}.$$

Dot $(\cdot)$ denotes differentiation with respect to the non-dimensional time $\tau = \omega_n t$. Depending upon the problem, the reference displacement x_0 can be suitably defined.

2.3. Control laws

The basic principle of the impulse damper, as discussed earlier, is to generate suitable impulsive forces by quickly expanding or contracting the PZT stack actuator. In the spirit of mimicking the most common dynamic mode of operation of an impact damper, these impulses should be generated at the instants of displacement zero-crossings of the primary mass. The stack is expanded by applying a suitable positive voltage across the PZT stack at the instants of the displacement zero-crossings with a positive velocity and a negative voltage is applied to contract the stack when the zero-crossings take place with a negative velocity. As the inherent damping of PZT stacks is generally very weak, rapid expansions and contractions of the actuator induce high-frequency transient oscillations. Such oscillations are highly undesirable and should be suppressed by an artificial damping. Depending upon the given situation, extra damping may be generated by velocity feedback or by some other electro-mechanical means, such as eddy-current damping. In what follows, damping is generated by velocity feedback. Moreover, sudden expansion and contraction is detrimental to the PZT stack that is generally very brittle. Therefore, expansion and contraction of the stack must allow certain finite duration in order to avoid severe shock. With these facts in mind, two basic control laws are proposed below:

2.3.1. Control law-I

The control law is mathematically recast as

$$\left.\begin{aligned} &V = V_1 + V_2 \\ &V_1 = V_1^+ H(\dot{X}) + V_1^- H(-\dot{X}) \\ &V_1^+ = \tfrac{2V_m}{\varepsilon}\left[XH(X) - (X-\varepsilon)H(X-\varepsilon) - \tfrac{\varepsilon}{2}\right] \quad \forall \dot{X} > 0 \\ &V_1^- = \tfrac{2V_m}{\varepsilon}\left[(X+\varepsilon)H(X+\varepsilon) - XH(X) - \tfrac{\varepsilon}{2}\right] \quad \forall \dot{X} < 0 \\ &V_2 = -\gamma \tfrac{\mathrm{d}Z}{\mathrm{d}\tau} \end{aligned}\right\}. \tag{22}$$

In Eq. (22), $H(\cdot)$ represents the usual Heaviside's step function that returns zero for semi-negative arguments and unity for positive arguments. ε is a positive (generally small) quantity that determines the zone of expansion and contraction of the actuator. The control function has two parts, of which the second part V_2 generates the damping force required to suppress unwanted transient oscillations of the stack. The first part of the control function V_1 is depicted in Fig. 3(a). Clearly, V_1 is hysteretic in nature. It has two branches each for a particular sign of the velocity of the primary system. The higher and the lower saturation limits of V_1 are $+V_m$ and $-V_m$, respectively. It may be noted that Fig. 3(a) assumes that $|X|_{\max} > \varepsilon$. However, as discussed

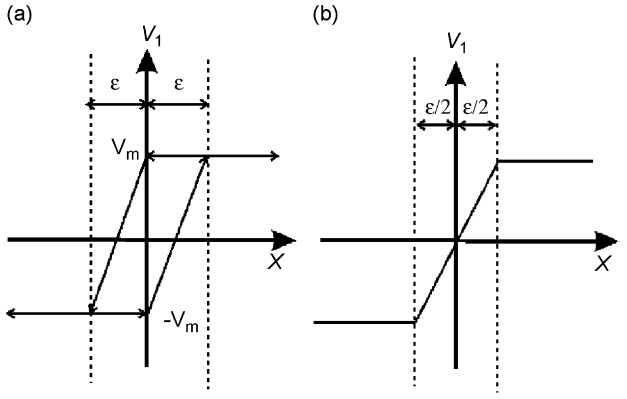

Fig. 3. Control laws for the proposed impulse damper.

elsewhere in the paper, when this control law is put into application, the maximum absolute displacement of the primary mass may fall below ε after some time and discontinuous jumps of the voltage are possible within the zone $|X|<\varepsilon$.

2.3.2. Control law-II

The first part of the control law-I being hysteretic in nature, the system response maybe oscillatory at the steady state, as shown later. A functionally simple, hysteresis-free form of V_1 is shown in Fig. 3(b) and is mathematically described as

$$V_1 = \begin{cases} V_m \operatorname{sgn}(X) & \forall |X| \geqslant \varepsilon/2, \\ \frac{2V_m}{\varepsilon} X & \forall |X| < \varepsilon/2. \end{cases} \tag{23}$$

It may be noted that in Eq. (23), the slope of the control function V_1 during switching is the same as in the control function (22). This allows one to compare the efficacies of the two control laws.

With the control functions defined above, system model (21) is rewritten as

$$\begin{bmatrix} 1 & 0 \\ r_m & r_m \end{bmatrix} \begin{Bmatrix} \ddot{X} \\ \ddot{Z} \end{Bmatrix} + \begin{bmatrix} 2\xi & -h_e \\ 0 & h_e \end{bmatrix} \begin{Bmatrix} \dot{X} \\ \dot{Z} \end{Bmatrix} + \begin{bmatrix} 1 & -\alpha \\ 0 & \alpha \end{bmatrix} \begin{Bmatrix} X \\ Z \end{Bmatrix} = \frac{\lambda^2}{1-\lambda^2} \alpha V_1 \begin{Bmatrix} -1 \\ +1 \end{Bmatrix}, \tag{24}$$

where $h_e = h_p + \lambda^2/(1-\lambda^2)\alpha\gamma$.

3. Stability of the controlled system

It is generally difficult to prove the absolute stability of the system. An indirect method is adopted here to analyse the dynamic characteristics of the system. It is sufficient to show that the system is dissipative and the free response of the primary system decreases with time. As the system is autonomous, the simplest form of the bounded instability of the equilibrium is identified with the existence of a stable limit cycle. Amplitude and frequency of the limit cycles in the present system can be approximately estimated as described below.

Fig. 4 depicts the block diagram of the control model (24) in frequency domain. In Fig. 4, $G(s)$, represents the linear fourth-order transfer function between V_1 and X where

$$b_2 = -\frac{\lambda^2}{1-\lambda^2}\alpha, \quad a_3 = 2\xi + (R_m+1)h_e, \quad a_2 = 1 + 2h_e\xi R_m + (1+R_m)\alpha,$$
$$a_1 = (h_e + 2\xi\alpha)R_m, \quad a_0 = \alpha R_m \quad \text{and} \quad R_m = \frac{1}{r_m}.$$

It is assumed that a periodic solution exists and this is approximated by $A\sin(\omega\tau)$. Frequency domain description of the nonlinear control function $V_1(X)$ can be given by the single input describing function (SIDF) [28] for a single-harmonic input of the form $X = A\sin(\omega\tau)$. Corresponding output of the nonlinear block is described as $V_1 = \hat{V}_0 \sin(\omega\tau + \phi)$. The complex describing function N of the nonlinear block is defined as

$$N = \frac{\hat{V}_0}{A} = \frac{1}{\pi A}\int_0^{2\pi} V_1(A\sin\theta)(\sin\theta + \mathrm{j}\cos\theta)\,\mathrm{d}\theta == N_r(A) + \mathrm{j}N_i(A), \tag{25}$$

where $\mathrm{j} = \sqrt{-1}$. $N_r(A)$ and $N_i(A)$ are real-valued functions of A.

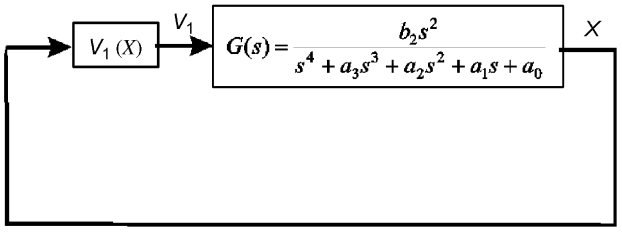

Fig. 4. Control model of impulse damper in frequency domain.

For the multivalued function V_1 given in Eq. (22), expressions for the SIDF can be obtained as

$$N_i(A) = -\frac{\Delta}{\pi A^2},$$
$$\Delta = \begin{cases} 2\varepsilon V_m, & A \geqslant \varepsilon, \\ 2\varepsilon V_m - \frac{2V_m}{\varepsilon}(\varepsilon - V_m)^2, & A < \varepsilon. \end{cases} \tag{26}$$

$$N_r(A) = \begin{cases} \frac{V_m}{\varepsilon}, & A < \varepsilon \\ \frac{1}{2\pi A}\int_0^{2\pi}\{V_1^+(A\sin\theta) + V_1^-(A\sin\theta)\}(\sin\theta)\,\mathrm{d}\theta = \frac{2V_m}{\varepsilon\pi}\left\{r\sqrt{1-r^2} + \sin^{-1}(r)\right\}, & A \geqslant \varepsilon \end{cases}.$$
$$r = \frac{\varepsilon}{A} \leqslant 1. \tag{27}$$

It may be noted that for the control function (23), $N_i(A) = 0$ and hence $N(A)$ is a real-valued function. The amplitude and frequency of the limit cycle can be estimated from the following equation:

$$G(\mathrm{j}\omega)N(A) = 1. \tag{28}$$

Thus, the existence of a limit cycle can be graphically confirmed by the existence of a point of intersection of the Nyquist plot $G(\mathrm{j}\omega)$ with the inverse SIDF plot $N^{-1}(A)$ in the complex plane and the corresponding values of ω and A, at the point of intersection, are the approximate estimates of the frequency and amplitude of the limit cycle. The estimated limit cycle is stable if the inverse SIDF plot crosses the Nyquist plot from right to left, as A increases, viewed along the direction of increasing ω [28].

The Nyquist plot of the linear part of the control system is shown in Fig. 5 for some typical parameter values. A zoomed view of the Nyquist plot near the origin is shown in inset-1. Intersection of the inverse SIDF, for the control law-I, with the Nyquist plot is depicted in inset-2. The intersection confirms the existence and stability of a limit cycle. There exists only a single point of intersection for a wide parameter region studied. Therefore, the system response approaches a stable limit cycle at the steady state. Fig. 6 shows the variation of the amplitude of the limit cycle with V_m for different values of h_e. From Fig. 6, it is observed that the limit cycle amplitude is in the order of ε and increases with V_m and decreasing h_e. Therefore, free vibration, initiated by a large perturbation ($\gg\varepsilon$), ultimately settles down to a low amplitude oscillation of $O(\varepsilon)$. Thus, the system response is decreasing and bounded for some parameter values. Existence of limit cycle oscillations is also confirmed by numerical simulations as shown in Fig. 7. It is observed that the frequency of the limit cycle is much higher than the natural frequency of the primary system. Even though, the amplitude of the residual oscillation of the primary system may be within the permissible value for some applications, such high-frequency oscillation may inflict damage to the actuator or excite higher-order modes of the primary system. Therefore, this high-frequency residual vibration must be eliminated from the system. This can be achieved in number of ways; one is to just switch off the actuator when the measured velocity at the zero-crossing goes down below a permissible threshold. Other useful methods are discussed below.

It may be noted that for the control law-II, the inverse SIDF plot is the entire positive real axis. Thus, the intersection of the SIDF plot with the Nyquist plot is possible only at the origin. Therefore, the control law-II renders the equilibrium attracting and hence stable.

3.1. Modified control law-I

With the objective of eliminating limit cycle oscillations in the system response, a slight modification of the control law-I is proposed below:

$$V_1 = \mathrm{Sat}(V_{11}, V_m),$$
$$V_{11} = \begin{cases} V_0 + \frac{2V_m}{\varepsilon}X & \forall X\dot{X} > 0, \quad |X| < \varepsilon, \\ V_0 & \text{otherwise}, \end{cases} \tag{29}$$

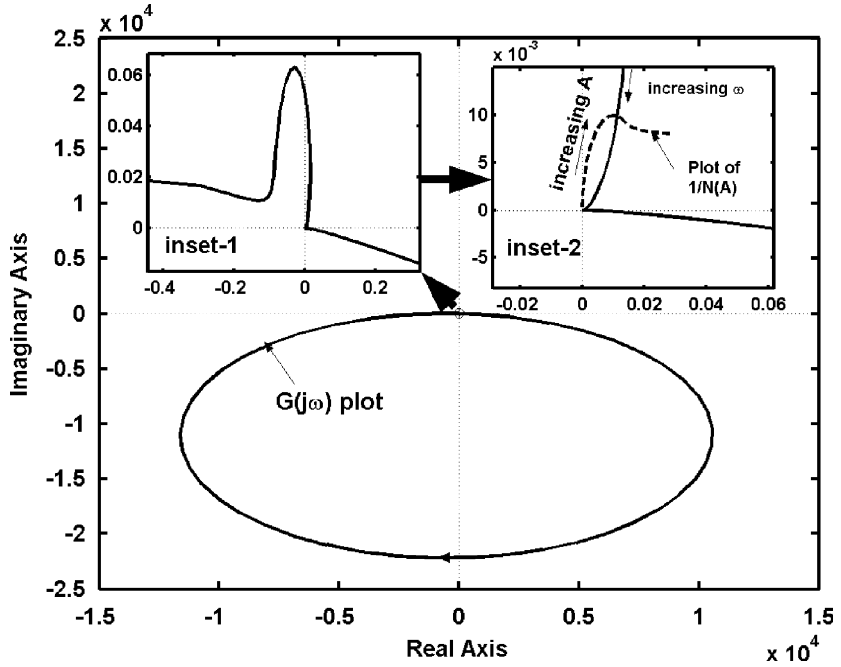

Fig. 5. Nyquist plot of the control system. $h_e = 5.0$, $V_m = 1$, $r_m = 0.1$, $\varepsilon = 0.1$, $\alpha = 100$, $\lambda = 0.7$, and $\xi = 0$.

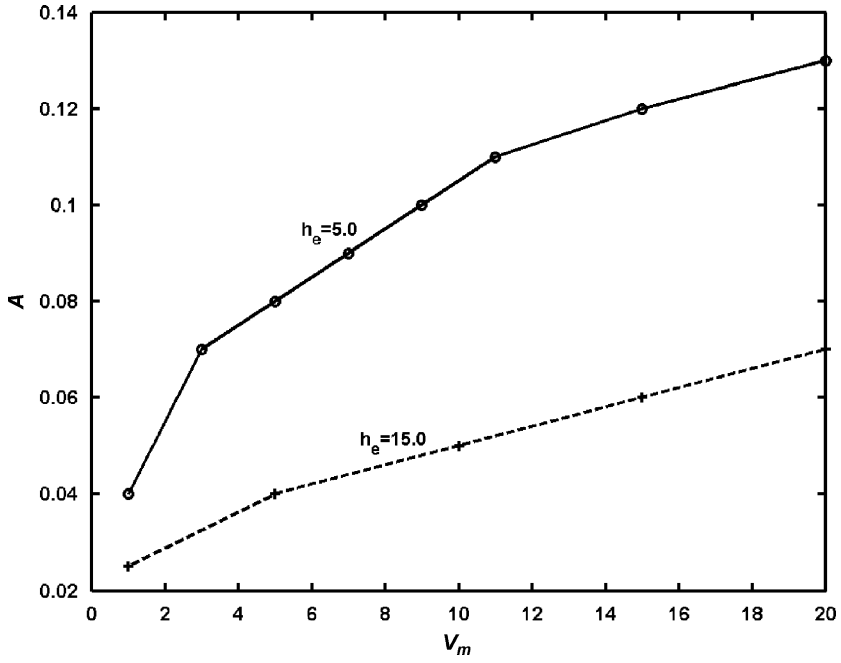

Fig. 6. Variation of the limit cycle amplitude with V_m. $r_m = 0.1$, $\varepsilon = 0.1$, $\alpha = 100$, $\lambda = 0.7$, and $\xi = 0$.

where $\mathrm{Sat}(u, v)$ represents saturation function that limits the value of u between $\pm v$. V_0 is the discrete variable updated to the value of V_{11} at each falling/rising edge of the trigger signal:

$$S = H(X\dot{X}(\varepsilon - |X|)). \tag{30}$$

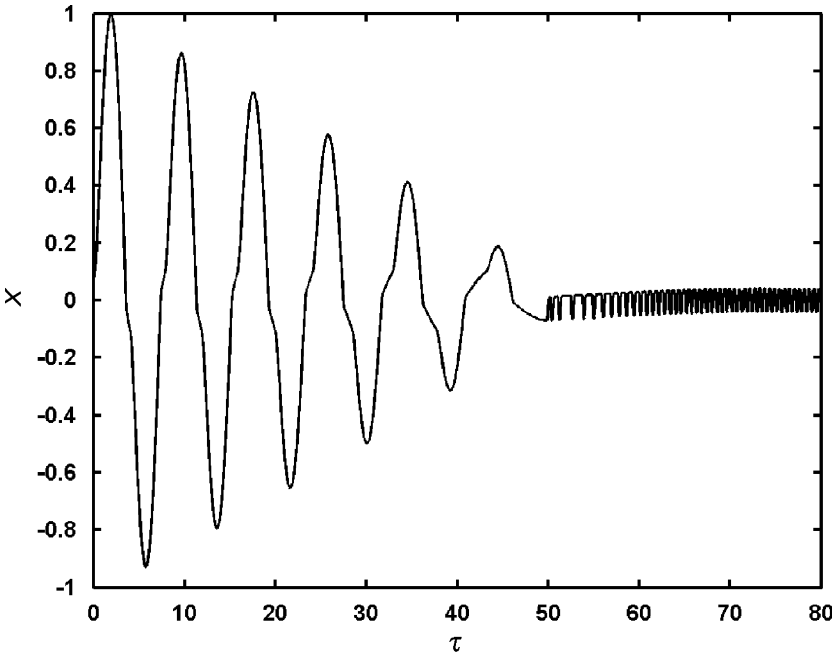

Fig. 7. Simulation result of free vibration with impulse damper with control law-I. $r_m = 0.1$, $\varepsilon = 0.1$, $\alpha = 100$, $\lambda = 0.7$, $\xi = 0$, $h_e = 25.0$, and $V_m = 3.0$.

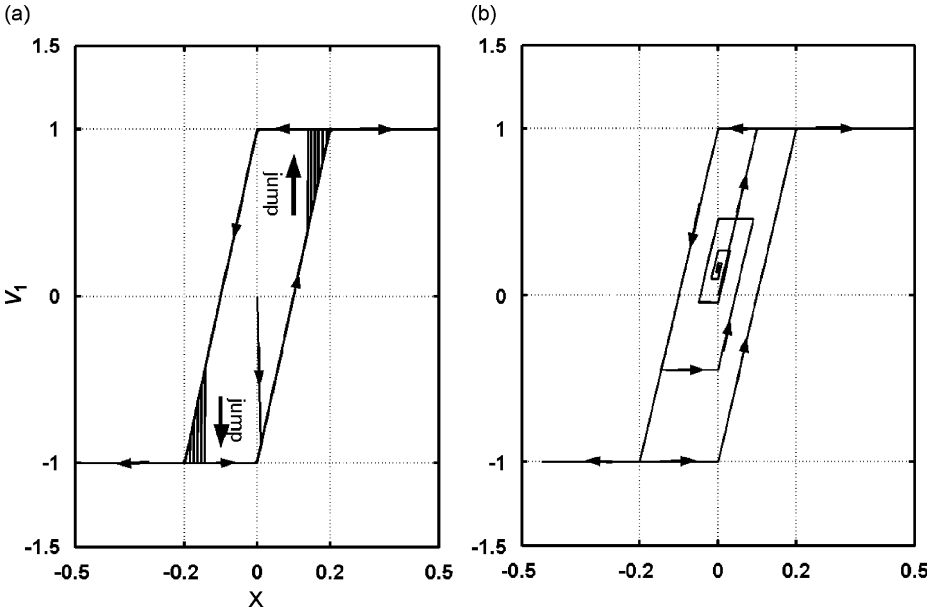

Fig. 8. Variation of control signal V_1 with displacement X. $V_m = 1.0$, $\varepsilon = 0.2$, $X = e^{-0.01\tau}\sin(\tau)$: (a) Control law-I and (b) modified control law-I.

Variations of the control signal V_1 with X, according to the control law-I and its modified version, are illustrated in Figs. 8(a) and (b), respectively. These plots are generated for an exponentially damped sinusoidal displacement X. Existence of the limit cycle oscillation in the system with the control law-I is ascribed to the persistence of the same maximum level (V_m) of the control signal V_1 even when the amplitude of X comes down below ε. This leads to the discontinuous jumps of the signal level V_1 at the peak values of X below ε. As mentioned earlier, Figs. 3(a) and 8(a) are different only in the respect that the discontinuous jumps of the

control force within the zone $|X|<\varepsilon$ are incorporated in Fig. 8(a). Obviously, for $|X|\geqslant\varepsilon$, the modified control law-I is equivalent to the control law-I. However, inside the region $|X|<\varepsilon$, the maximum value of V_1 decreases with X and eventually, V_1 approaches a constant value with X going down to zero. From Fig. 8(b), it can be observed that the control signal assumes a non-trivial value at the steady state. This does not pose any great problem in practice because the actuator can be switched off after the free vibration subsides.

4. Controlling free vibration

Stability analysis discussed above does not shed any light on the efficacy of the system as a damper. In what follows, efficacy of the two control laws in attenuating free vibrations are analysed and compared with the results of numerical simulations. For this purpose, a MATLAB SIMULINK model is developed based on Eq. (24). Numerical integration of the model is carried out using the Dormand–Prince algorithm (ode45 routine of MATLAB). As an initial excitation to the system, the initial velocity of the primary mass is set to v_0, which again by the suitable choice of x_0 is scaled to unity, i.e., $v_0 = 1$. Acknowledging the fact that the stiffness of the PZT stack actuator is a few orders higher than the usual stiffness of the primary system, the stiffness ratio α is set to 100. As the primary system is lightly damped, inherent damping of the primary system is considered zero, i.e., $\xi = 0$. Following parameters are close to the practically feasible values: $\lambda = 0.7$, $r_m = 0.1$.

Numerically simulated time histories are shown in Figs. 9 and 10 for the modified control law-I and control law-II, respectively. From these figures, the decay of the free vibration is apparent. Comparing Figs. 9(a) and 10(a), it may be concluded that for the same parameter values, the modified control law-I is more efficient.

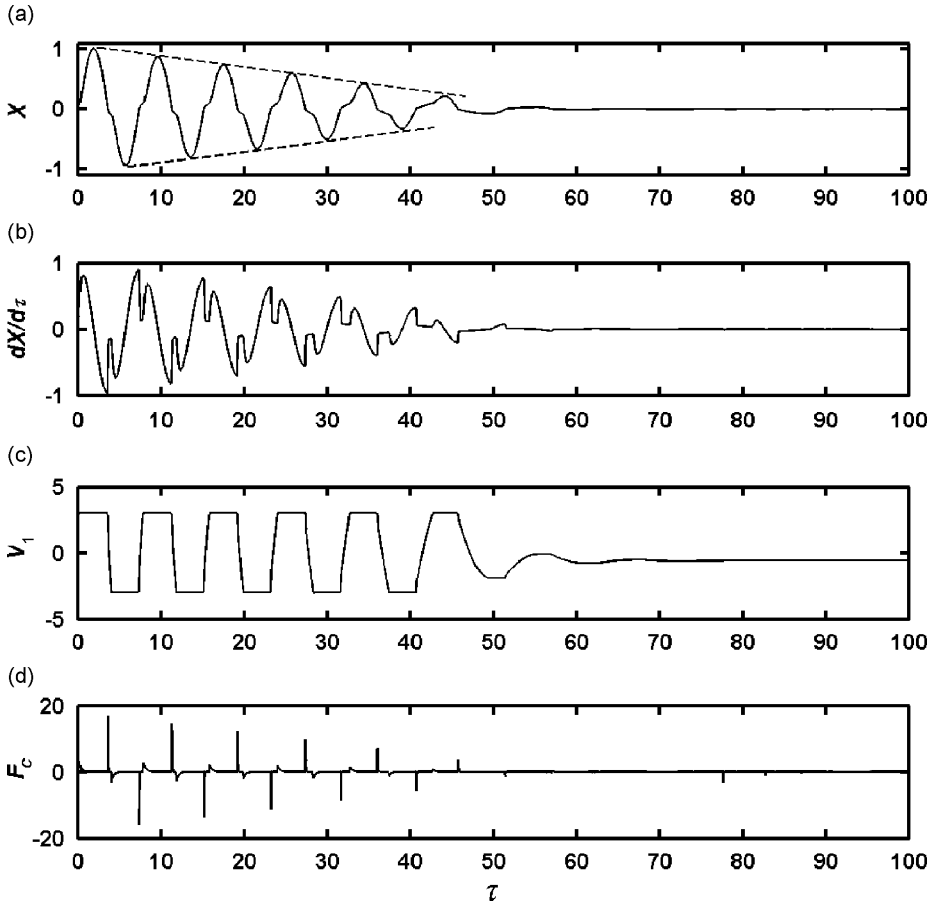

Fig. 9. Free vibration time history with the modified control law-I. $r_m = 0.1$, $\varepsilon = 0.1$, $\alpha = 100$, $\lambda = 0.7$, $\xi = 0$, $h_e = 25.0$, and $V_m = 3.0$.

The effective control effort acting on the primary system may be defined as

$$F_c = \alpha Z + h_e \dot{Z} - \frac{\lambda^2}{1-\lambda^2}\alpha V_1. \tag{31}$$

Figs. 9(d) and 10(d) show the time history plots of the effective control efforts acting on the primary mass for the modified control law-I and control law-II, respectively. From these figures, it is clearly observed that the control efforts acting on the primary system are nothing but a series of impulses.

The major parameters that have substantial influence on the performance of the damper are h_e, V_m, and ε. Suitable performance indices of the damper are the rate of decay and the decay time of the free response. From Figs. 9(a) and 10(a), it is observed that the initial decay envelopes are linear for the chosen parameter values. For other parameter values, the decay envelopes are found to be more complex. Decay envelopes for various parameter values are plotted in Figs. 11(a)–(c). However, as the initial part of the decay is always found to be linear, the initial decay rate, defined as the absolute value of the slope of the initial decay envelope, may be a good measure of the amount of damping generated by the damper. Variations of the initial decay rate with h_e and V_m are shown in Figs. 12(a) and (b) for the modified control law-I and control law-II, respectively. It is observed that the initial decay rate increases with h_e and V_m. It is already noted that the modified control law-I is more efficient compared to the control law-II. This is further confirmed by comparing Figs. 12(a) and (b). Therefore, the control law-II is not explored further.

It is established that the control efforts on the primary system are impulsive in character. The characteristics of the impulses depend on the rate at which the PZT actuator is expanded or contracted. With the maximum level of the control signal (V_m) and the other parameter values fixed, the rate of contraction and expansion depends mainly on ε. Thus, it is pertinent to explore the effect of ε on the rate of decay. Fig. 13 shows the

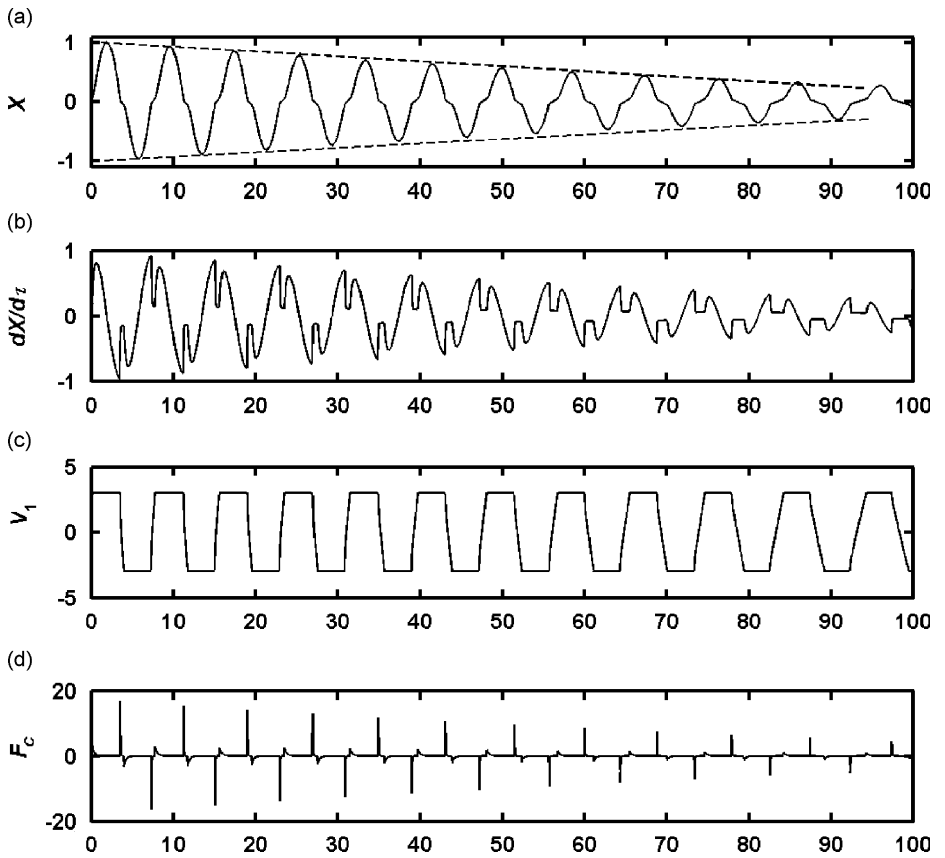

Fig. 10. Simulation result of free vibration with impulse damper with control law-II. $r_m = 0.1$, $\varepsilon = 0.1$, $\alpha = 100$, $\lambda = 0.7$, $\xi = 0$, $h_e = 25.0$, and $V_m = 3.0$.

variation of the initial decay rate with ε. The existence of an optimum value of ε for obtaining the maximum decay rate (initial) is apparent from these plots.

Despite the initial decay rate is a feasible measure of the amount of damping produced by the damper, it is not a good measure of the overall performance of the damper. In fact, decay changes with time and thus,

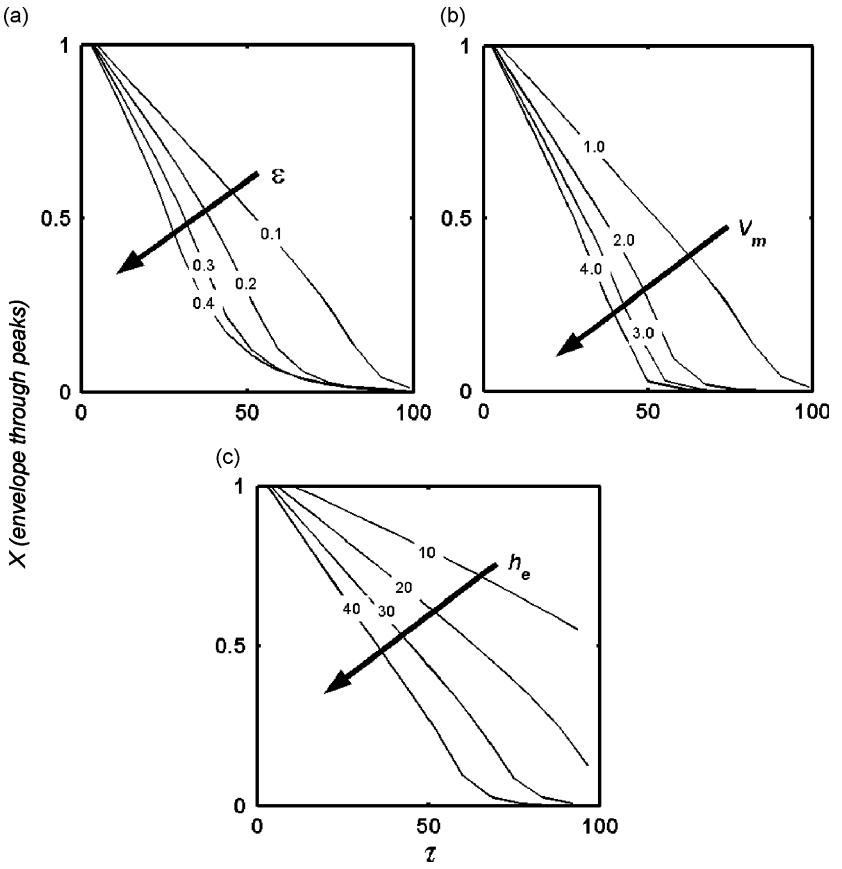

Fig. 11. Decay envelopes for the modified control law-I. $r_m = 0.1$, $\alpha = 100$, $\lambda = 0.7$, $\xi = 0$: (a) $h_e = 25$, $V_m = 1.0$; (b) $h_e = 25$, $\varepsilon = 0.1$; and (c) $V_m = 1.0$, $\varepsilon = 0.1$.

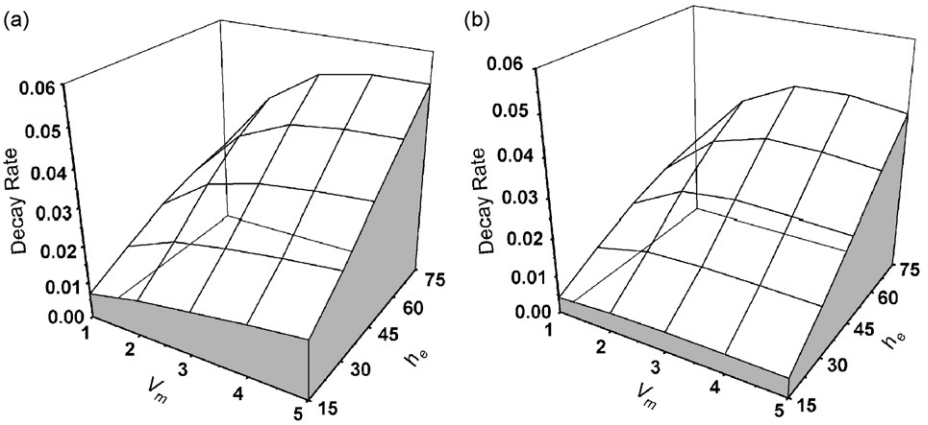

Fig. 12. Plots of the initial decay rate with V_m and h_e. $r_m = 0.1$, $\varepsilon = 0.1$, $\alpha = 100$, $\lambda = 0.7$, $\xi = 0$: (a) Modified control law-I and (b) control law-II.

decay time is another good measure of the overall performance of the damper. In what follows, two different types of decay time estimates are considered:

A. *Displacement criterion*: The time traversed before the displacement response of the primary system becomes permanently less than a predefined value x_d, generally low. Here, $x_d = 0.05$ is used.
B. *Energy criterion*: The time traversed before the initial energy of the primary system permanently goes below a predefined value E_d. Here, $E_d = 0.01$ is used.

Variations of the decay time with ε are shown in Figs. 14(a)–(d) for various parameter values. Clearly, optimum values of ε that minimizes the decay time can be found.

5. Controlling forced vibration

Efficacy of the proposed impulse damper in controlling the free vibration of a single-degree-of-freedom primary system has been established in Section 4. The damper can as well be used to control forced vibration. Numerical simulations are carried out for a random external disturbance acting on the primary mass. The random external excitation is generated by filtering uniformly distributed random numbers between $[-R, R]$ through an analogue Butterworth band-pass filter of order 8. R is scaled to unity by properly selecting the reference displacement x_0. The frequency spectrum of the generated random input is shown in Fig. 15(a). The system is numerically integrated using the Dormand–Prince algorithm (ode45). Integration is carried out for some time without the damper and then the damper is engaged. The time domain responses of the primary mass are shown in Figs. 15(c) and (d) for two different values of h_e. From Figs. 15(b) and (c) and the frequency domain response, Fig. 15(d), the efficacy of the damper in controlling the forced vibration is apparent. The role of h_e is important to note from the frequency domain response shown in Fig. 15(d). For relatively lower values of h_e, the response in the intermediate high-frequency range is increased by the damper. This is imputed to the transient ringing of the PZT actuator during expansions and contractions. Higher value of h_e can control this ringing as apparent from the reduced response in the high-frequency range.

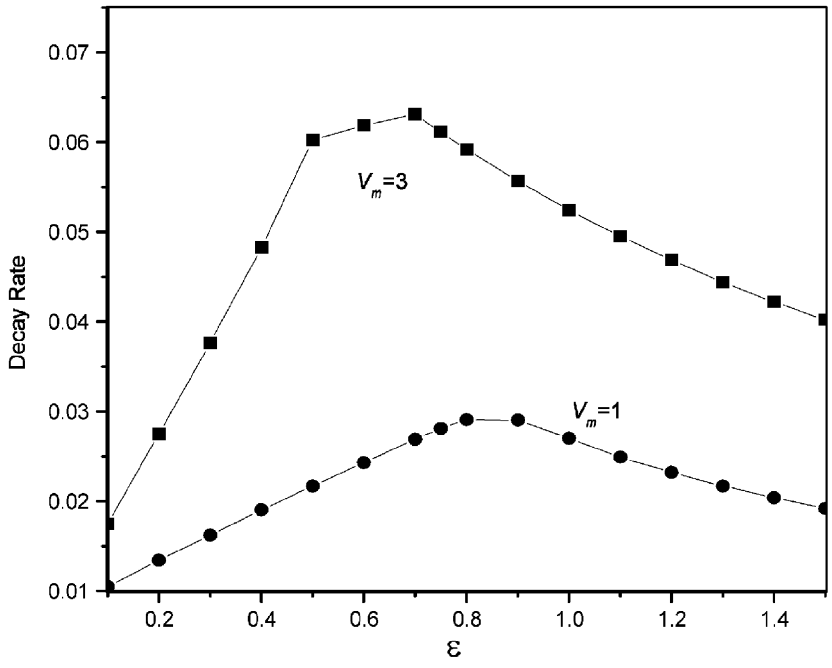

Fig. 13. Variation of the initial decay rate with ε for modified control law-I. $h_e = 25$, $r_m = 0.1$, $\varepsilon = 0.1$, $\alpha = 100$, $\lambda = 0.7$, $\xi = 0$.

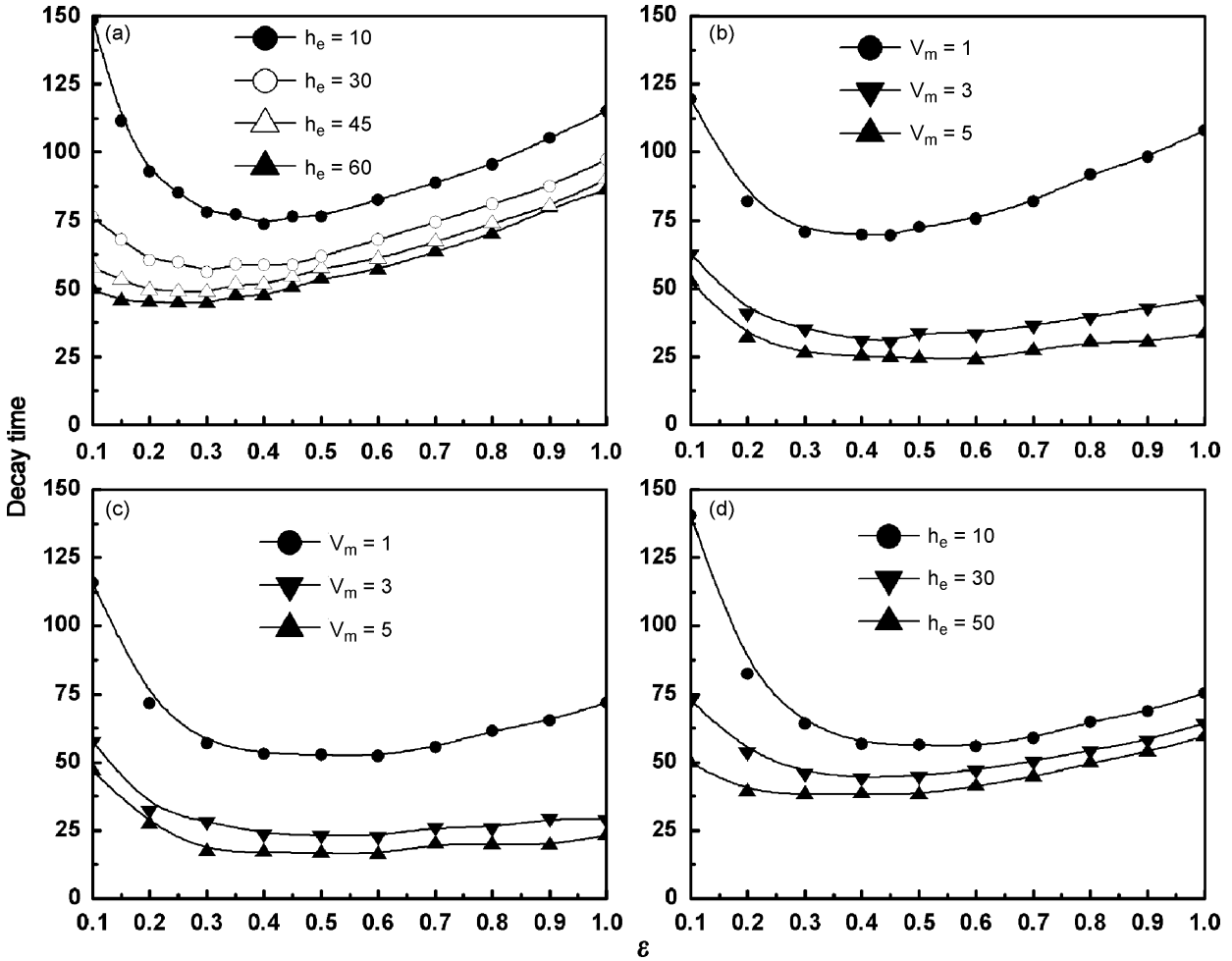

Fig. 14. Variation of decay time with ε: (a, b) displacement criterion and (c, d) energy criterion. $r_m = 0.1$, $\alpha = 100$, $\lambda = 0.7$, $\xi = 0$. (a, d) $V_m = 1.0$; (b, c) $h_e = 15$.

Numerical simulations are also carried out to explore the effect of a single damper on a two-degrees-of-freedom primary system. Both resonance peaks are controlled by a single damper. Results are not presented here to conserve space.

6. Controlling self-excited vibration

In this section, role of the proposed damper in controlling self-excited vibration is explored. The following non-dimensional model of the system is considered for simulation:

$$\begin{bmatrix} 1 & 0 \\ r_m & r_m \end{bmatrix} \begin{Bmatrix} \ddot{X} \\ \ddot{Z} \end{Bmatrix} + \begin{bmatrix} 0 & -h_e \\ 0 & h_e \end{bmatrix} \begin{Bmatrix} \dot{X} \\ \dot{Z} \end{Bmatrix} + \begin{bmatrix} 1 & -\alpha \\ 0 & \alpha \end{bmatrix} \begin{Bmatrix} X \\ Z \end{Bmatrix} + \begin{Bmatrix} f_s(X, \dot{X}) \\ 0 \end{Bmatrix} = \frac{\lambda^2}{1-\lambda^2} \alpha V_1 \begin{Bmatrix} -1 \\ +1 \end{Bmatrix} + \begin{Bmatrix} w(\tau) \\ 0 \end{Bmatrix}, \tag{32}$$

where the nonlinear function f_s describes the self-exciting force and is considered here as

$$f_s(X, \dot{X}) = -a(\dot{X} - b\dot{X}^3), \tag{33}$$

where a and b are two positive real parameters.

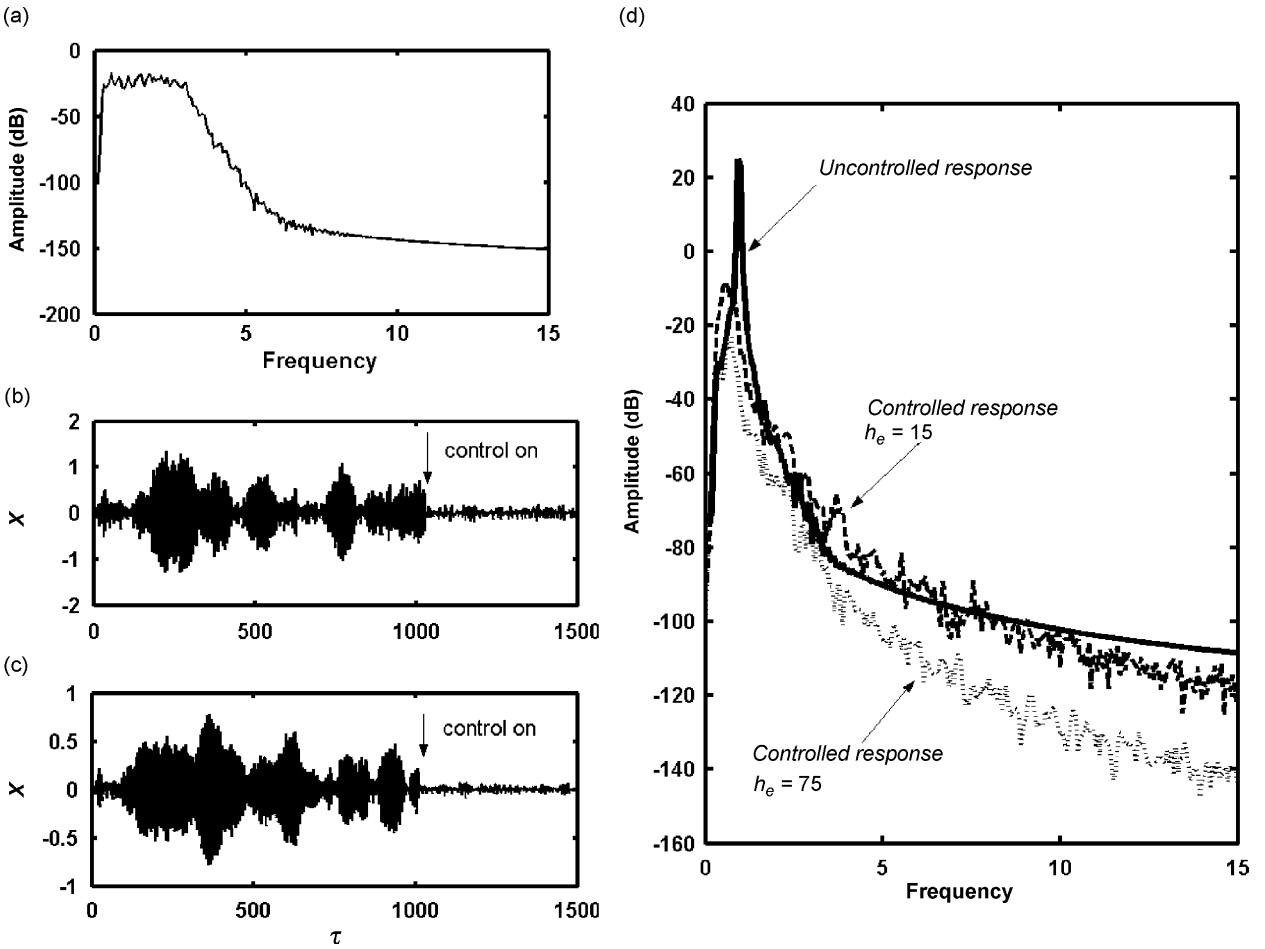

Fig. 15. Forced response of the system with and without impact damper. $r_m = 0.1$, $\alpha = 100$, $\lambda = 0.7$, $\xi = 0.005$, $V_m = 5.0$, $\varepsilon = 0.4$: (a) Frequency spectrum of the excitation; (b) time domain response for $h_e = 15$; (c) time domain response for $h_e = 75$; and (d) frequency domain response. Modified control law-I is used.

$w(\tau)$ is the random external excitation acting on the primary system. Results of the numerical simulations for $w(\tau) = 0$ are shown in Figs. 16(a)–(d). Initially, integrations are run for $\tau = 0$–250 without the damper engaged and then the damper is switched on. The system being driven by the self-exciting force f_s settles down to a periodic vibration. Figs. 16(a)–(d) confirm that this self-excited vibration can be controlled by the proposed damper. Comparing Figs. 16(a) and (c), it may be concluded that self-excited vibration may be controlled to a great extent (though complete quenching is theoretically not possible) by properly selecting the value of ε. Similar comparison between Figs. 16(a) and (b) reveals that the amplitude of self-excited vibration can be progressively reduced by increasing the value of V_m. Comparing Figs. 16(b) and (d), it may be inferred that the increasing value of h_e has a favourable influence on the response of the controlled system.

Efficacy of the proposed damper is further demonstrated for a more complex situation where the self-excited system is externally excited by a random disturbance. The random excitation $w(\tau)$ is generated by post-filtering uniformly distributed random numbers between $[-R_w, R_w]$ by an analogue Butterworth band-pass filter of order 8 with the pass-band frequency range [0.5, 2]. R_w is scaled to 10 by properly selecting the reference displacement x_0. $w(\tau)$, thus generated, is shown in Fig. 16(f). Integration is carried out for $\tau = 0$–500 without the damper and then the damper is engaged to control the vibration. Time history plot of the system response is shown in Fig. 16(e), which demonstrates the damper's efficaciousness. It is observed that the amplitude of response is small for most of the time, albeit intermittent amplitude fluctuations are present.

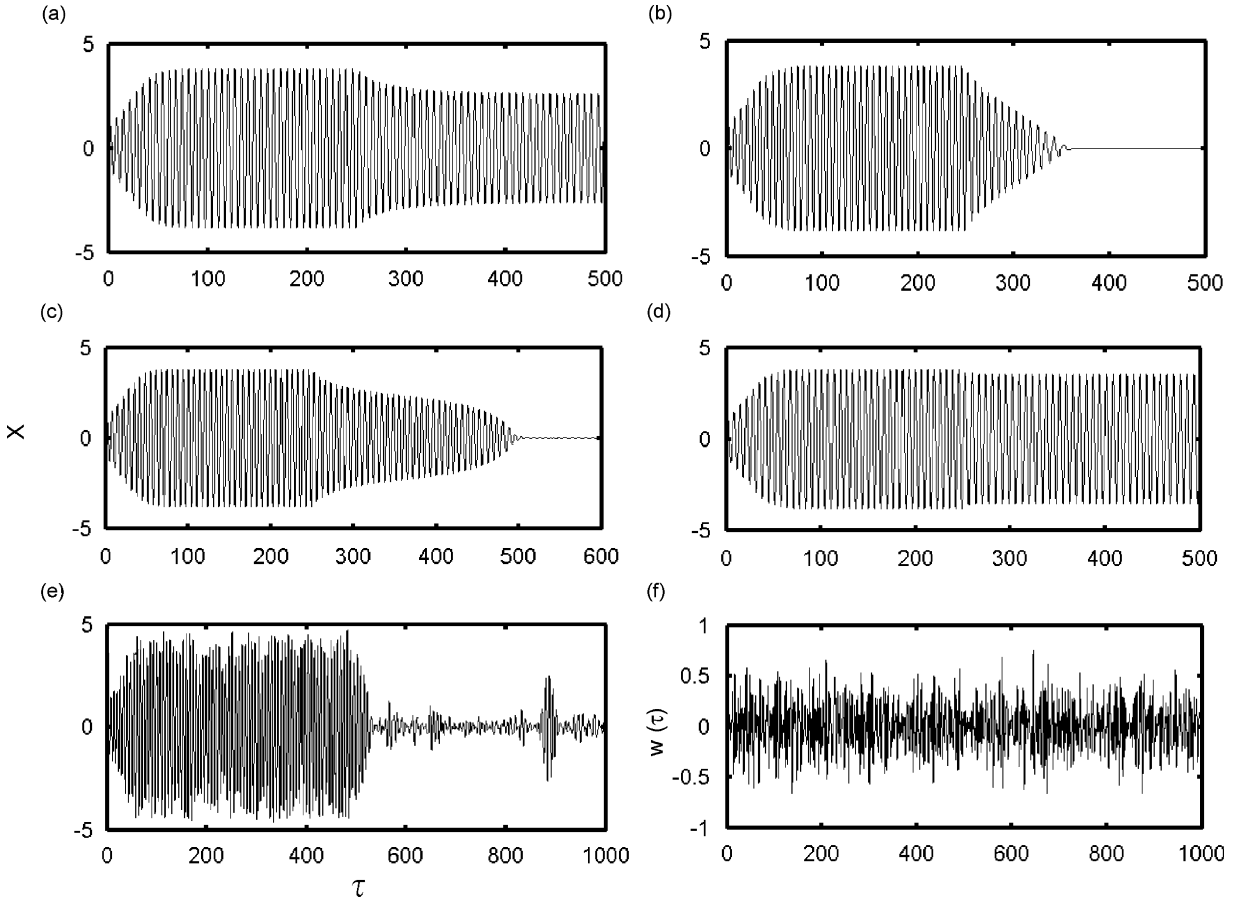

Fig. 16. Response of self-excited system with and without impulse damper. $r_m = 0.1$, $\alpha = 100$, $\lambda = 0.7$, $a = 0.1$, $b = 0.1$: (a–d) without external excitation; (e) with external random excitation; (f) external excitation: (a) $V_m = 3.0$, $\varepsilon = 0.1$, $h_e = 75$; (b) $V_m = 5.0$, $\varepsilon = 0.1$, $h_e = 75$; (c) $V_m = 3.0$, $\varepsilon = 0.4$, $h_e = 75$; (d) $V_m = 5.0$, $\varepsilon = 0.1$, $h_e = 30$; and (e) $V_m = 5.0$, $\varepsilon = 0.4$, $h_e = 100$. Modified control law-I is used.

However, no specific reasons can be attributed to these intermittent fluctuations. Possibly, it is due to some complex interaction of nonlinearity of the primary system and the random external excitation. Indeed, increasing the voltage level reduces these amplitude fluctuations.

7. Dynamic control law

In the foregoing, it is established that the vibration of a single-degree-of-freedom system can be controlled by series of impulses generated due to the expansions and contractions of a mass loaded PZT stack actuator. The basic control algorithms, fundamentally conceived from the principle of impact dampers, are consisting of two parts. The first part of the control function provides damping in the PZT actuator. The second part commands the expansion and contraction of the actuator based on the state of the primary system. The hysteretic controller proves to be more efficacious compared to the non-hysteretic controller. The modified control law-I is only one example out of many possibilities of realizing the controller. The hysteretic part [29] of the controller can alternatively be realized using the following simple dynamic control law:

$$V_1 = K_h \Phi, \tag{34}$$

where Φ is obtained as

$$\dot{\Phi} = \mu X(1 - \mathrm{sign}(X)\Phi). \tag{35}$$

The real parameter μ controls the shape and the size of the hysteresis curve, and K_h is the gain of the controller. It is easy to see that $-1 \leqslant \Phi \leqslant 1$, and Φ is frequency dependent. Effects of the parameter μ and the frequency of operation on the hysteretic behaviour of Φ are illustrated in Fig. 17 for different sinusoidal inputs. Numerically simulated time histories of the free vibration with the above controller are plotted in Figs. 18 and 19 for two different controller gains. It is observed that the performance of the controller can be improved by increasing the controller gain. Thus, in real life applications, substantial reduction in vibration can be achieved by adaptively tuning the controller gain. Forced vibration response of the system, under the same input as illustrated in Fig. 15(a), is plotted in Fig. 20, which demonstrates the efficacy of a dynamic controller for the impulse damper.

It is noteworthy that the dynamic controller uses only the information of a single state (X) of the primary system, whereas the control law-I and its modified version use the information of both displacement and velocity of the primary system. However, practical realization of the dynamic control law is somewhat more complex. Moreover, the hysteretic behaviour of the dynamic control law being rate dependent (unlike the modified control law-I, which is rate independent), one should carefully choose the parameter μ depending upon the operating range of frequencies. Of course, when the controller is used in adaptive mode, this is not of any serious concern.

8. Conclusions

In the present article, feasibility of a novel and active method of controlling vibration is proposed. The basic mechanism mimics the best mode of functioning of an impact damper in a more flexible and versatile way.

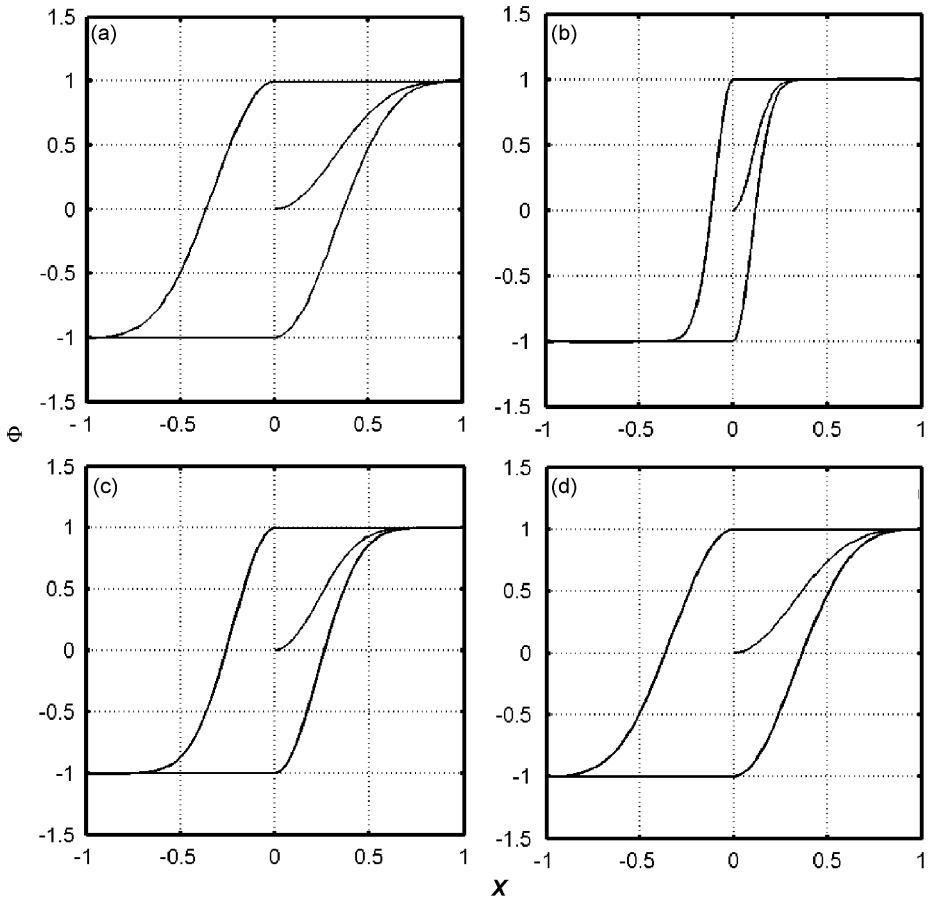

Fig. 17. Hysteresis plots Φ vs. X: (a) $\mu = 10$, $X = \sin(\tau)$; (b) $\mu = 100$, $X = \sin(\tau)$; (c) $\mu = 100$, $X = \sin(5\tau)$; and (d) $\mu = 100$, $X = \sin(10\tau)$.

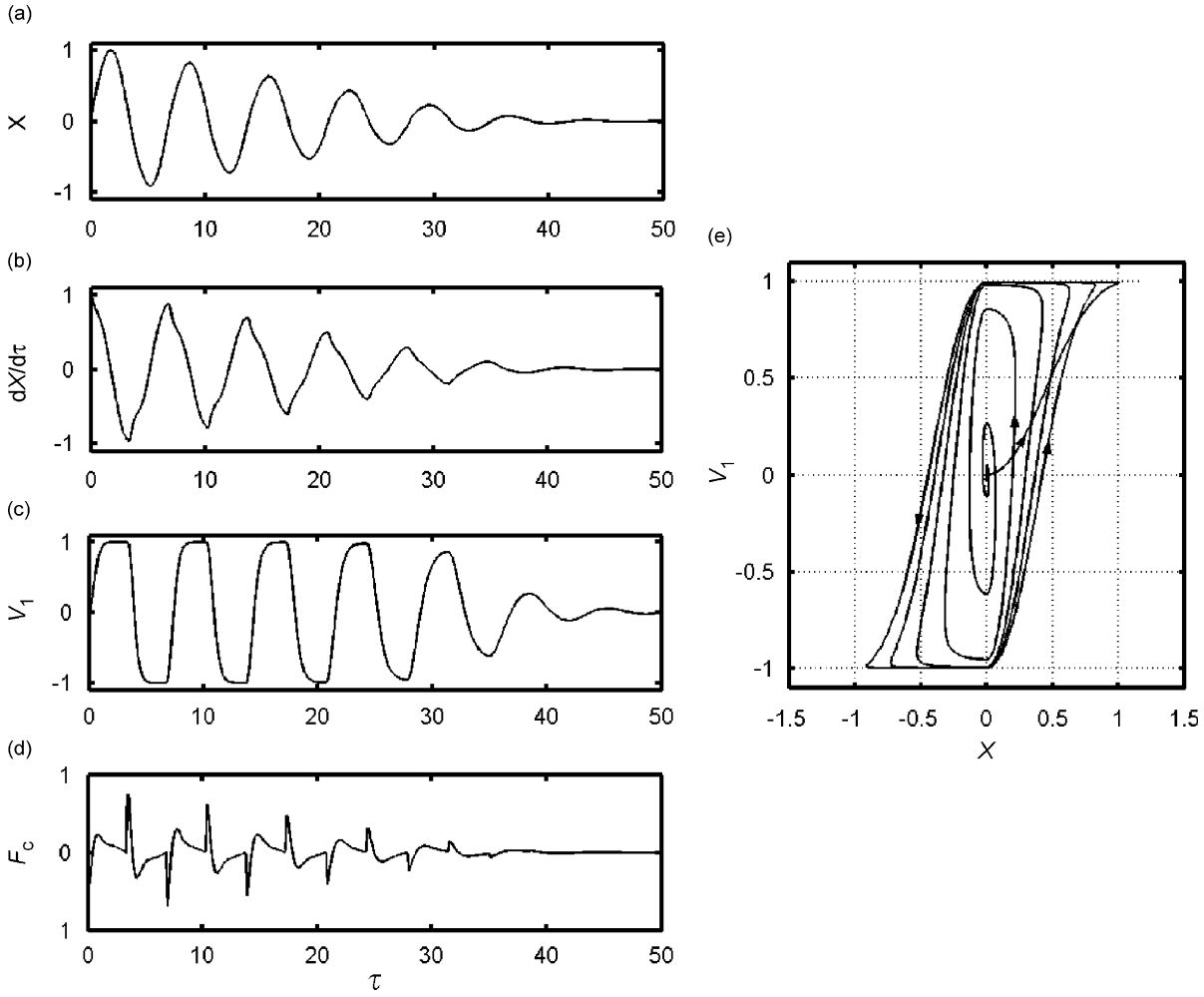

Fig. 18. Numerically simulated time history plots with the dynamic controller given by Eqs. (34) and (35). $r_m = 0.1$, $\alpha = 100$, $h_e = 5$, $\xi = 0$, $\mu = 5$, and $K_h = 1.0$.

In the proposed method, controlled impulses, generated by expanding and contracting a mass loaded PZT actuator, replace mechanical collisions between the primary system and the secondary masses. Thus, the proposed system has the merit of becoming a silent and soft substitute of impact dampers. Moreover, the requirements of physical impacts, a loose mass, and a cavity in the primary system are circumvented.

The basic principle of the damper is demonstrated for a single-degree-of-freedom model of the primary system. Two different types of static control laws are discussed and compared with respect to their efficacies in attenuating vibration. The control laws are conceived with the objective of expanding and contracting the actuator at suitable states of the primary system without the requirement of an explicit knowledge of the global dynamics of the system. Thus, the control laws are robust in a sense that the success of these laws do not depend on any explicit model of the system dynamics. The hysteretic control law is found to be more efficient in attenuating vibration.

Efficacies of the proposed damper are studied for controlling the free vibration, forced vibration under broadband random excitations, and the self-excited vibration with and without external excitations. It is shown that the damper can control the vibration in each of these simple to complex situations. Effects of different parameters of the controller are studied and it is shown that the performance of the damper can be optimized by suitable choice of the control parameters. Thus, the proposed system can be used in an

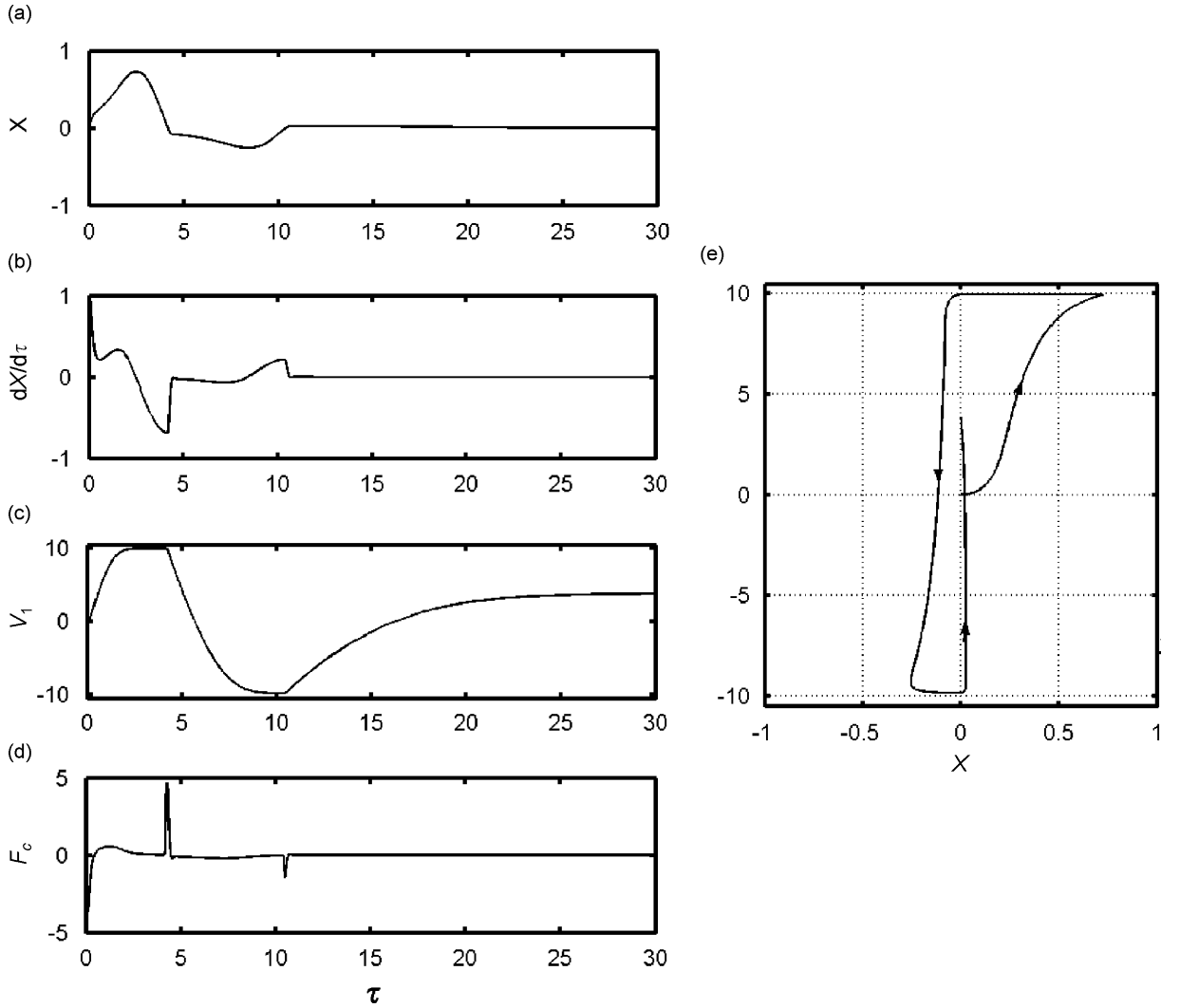

Fig. 19. Numerically simulated time history plots with the dynamic controller given by Eqs. (34) and (35). $r_m = 0.1$, $\alpha = 100$, $h_e = 5$, $\xi = 0$, $\mu = 5$, and $K_h = 10$.

adaptive way to control vibrations of lightly damped flexible structures without any explicit knowledge of the system model.

The use of dynamic control law to generate the hysteretic control commands for expanding and contracting the actuator is also considered. In the dynamic control law, the hysteretic part of the control command is governed by a first-order nonlinear ODE.

A conventional active vibration control system utilizes full/partial state feedback and often the control law demands the estimation of the model of the system. Successful estimation of the model calls for sufficient prior information regarding the global dynamic characteristics of the primary system. Thus, the range of applicability of the conventional active control system is rather limited. However, the strongest advantage of the proposed scheme is that the control law does not assume any particular model of the system and only the instants of the zero-crossings of the displacement of the primary system are required. Thus, in principle, measurements, or estimation of the states (except in the case of the dynamic control law), as well as a mathematical model of the system, is not required for the successful operation of the control. Various examples have amply demonstrated that a single control law is capable of controlling the vibration of a large class of systems.

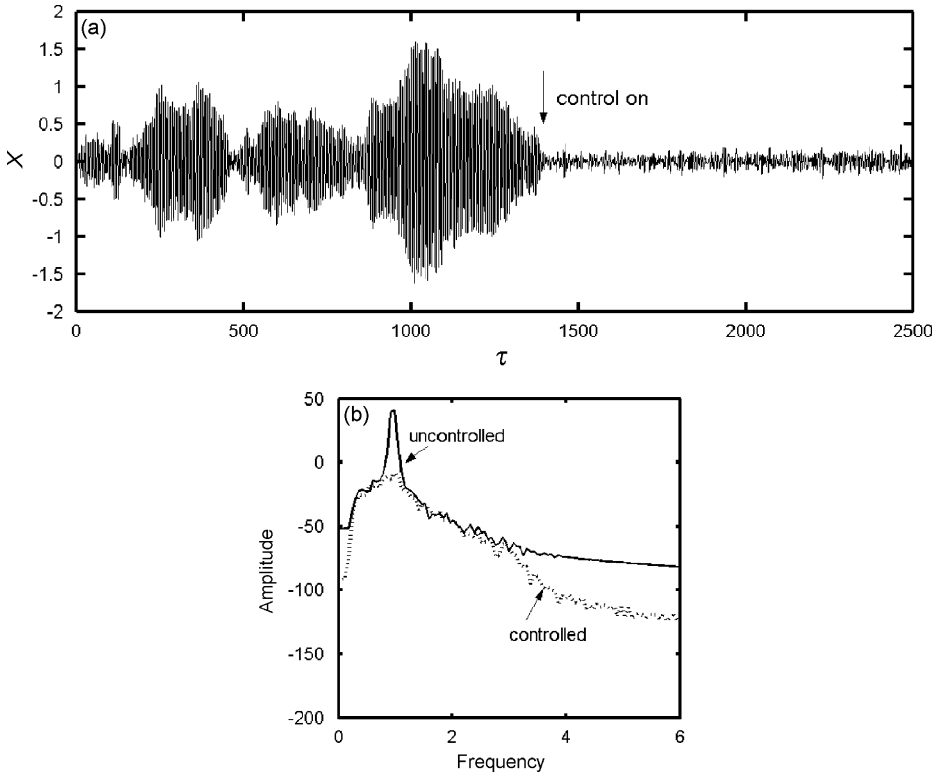

Fig. 20. Forced vibration response with the dynamic controller. $r_m = 0.1$, $\alpha = 100$, $\lambda = 0.7$, $\xi = 0.005$, $h_e = 25$, $K_h = 1$, $\mu = 5$: (a) displacement time history of the primary system and (b) frequency response plot.

Finally, it may be mentioned that as the proposed system utilizes a PZT actuator, the compactness of the actuator allows the proposed method to be practically implemented in various length scales ranging from macro- to microsystems, for example, vibrating structures in microelectromechanical systems and various other micromachines.

References

[1] A.L. Paget, Vibration in steam turbine buckets and damping by impacts, *Engineering* 143 (1937) 305–307.
[2] C. Grubin, On the theory of acceleration damper, *Journal of Applied Mechanics* 23 (1956) 373–378.
[3] G. Warburton, On the theory of acceleration damper, *Journal of Applied Mechanics* 24 (1957) 322–324.
[4] S.F. Masri, T.K. Caughey, On the stability of the impact damper, *Journal of Applied Mechanics—Transactions of the American Society of Mechanical Engineers* E33 (1966) 586–592.
[5] S.F. Masri, General motion of impact dampers, *Journal of the Acoustical Society of America* 47 (1970) 229–237.
[6] C.N. Bapat, S. Sankar, N. Popplewell, Experimental investigation of controlling vibrations using multi-unit impact damper, *Shock and Vibration Bulletin* 4 (1983) 1–12.
[7] C.N. Bapat, S. Sankar, Single unit impact damper in free and forced vibration, *Journal of Sound and Vibration* 99 (1985) 85–94.
[8] S. Chatterjee, A.K. Mallik, A. Ghosh, Impact dampers for controlling self-excited oscillation, *Journal of Sound and Vibration* 193 (5) (1996) 1003–1014.
[9] K.R. Asfar, S.N. Akour, Optimization analysis of viscous impact damper for controlling self-excited vibrations, *Journal of Vibration and Control* (2004) preprint.
[10] B. Blazejczyk-Okolewska, Analysis of an impact damper of vibration, *Chaos, Solitons and Fractals* 12 (2001) 1983–1988.
[11] P. František, More detail view on the dynamics of the impact damper, *FACTA UNIVERSITATIS Series: Mechanics, Automatic Control and Robotics* 3 (2003) 907–920.
[12] A. Papalou, S.F. Masri, Response of impact dampers with granular materials under random excitation, *Earthquake Engineering and Structural Dynamics* 25 (1996) 253–267.
[13] K.P. Duffy, R.L. Bagley, O. Mehmed, On a self-tuning impact vibration damper for rotating turbomachinery, *NASA/TM-2000-210215*, 2000, available electronically at 〈http://gltrs.grc.nasa.gov/GLTRS〉.

[14] S. Chatterjee, A.K. Mallik, A. Ghosh, On impact dampers for nonlinear vibrating systems, *Journal of Sound and Vibration* 187 (3) (1995) 403–420.
[15] K. Li, A.P. Darby, An experimental investigation into the use of a buffered impact damper, *Journal of Sound and Vibration* 291 (2006) 844–860.
[16] M.R. Duncan, C.R. Wassgren, C.M. Krousgrill, The damping performance of a single particle impact damper, *Journal of Sound and Vibration* 286 (2005) 123–144.
[17] S.L.T. de Souza, I.L. Caldas, R.L. Viana, J.M. Balthazar, R.M.L.R.F. Brasil, Impact dampers for controlling chaos in systems with limited power supply, *Journal of Sound and Vibration* 279 (2005) 955–967.
[18] Zhiwei Xu, Michael Yu Wang, Tianning Chen, Particle damping for passive vibration suppression: numerical modelling and experimental investigation, *Journal of Sound and Vibration* 279 (2005) 1097–1120.
[19] C.C. Cheng, J.Y. Wang, Free vibration analysis of a resilient impact damper, *International Journal of Mechanical Sciences* 45 (2003) 589–604.
[20] M. Saeki, Impact damping with granular materials in a horizontally vibrating system, *Journal of Sound and Vibration* 251 (1) (2002) 153–161.
[21] S. Ema, E. Marui, Suppression of chatter vibration of boring tools using impact dampers, *International Journal of Machine Tools and Manufacture* 40 (2000) 1141–1156.
[22] S.F. Masri, R.K. Miller, T.J. Deghanyar, T.K. Caughey, Active parameter control of nonlinear vibrating structures, *Journal of Applied Mechanics—Transactions of the American Society of Mechanical Engineers* 56 (1989) 658–666.
[23] S.F. Masri, G.A. Bekey, T.K. Caughey, Optimum pulse control of flexible structures, *Journal of Applied Mechanics—Transactions of the American Society of Mechanical Engineers* 48 (1981) 619–626.
[24] S.F. Masri, G.A. Bekey, T.K. Caughey, Online control of nonlinear flexible structures, *Journal of Applied Mechanics—Transactions of the American Society of Mechanical Engineers* 49 (1982) 877–884.
[25] F.E. Udwadia, S. Tabaie, Pulse control of single degree-of-freedom systems, *Journal of the Engineering Mechanics Division—ASCE* 107 (1981) 997–1009.
[26] F.E. Udwadia, S. Tabaie, Pulse control of structural and mechanical systems, *Journal of the Engineering Mechanics Division—ASCE* 107 (1981) 1011–1028.
[27] Han J.M.T.A. Adriaens, W.L. de Koning, R. Banning, Modelling piezoelectric actuators, *IEEE/ASME Transactions on Mechatronics* 5 (4) (2000) 331–341.
[28] P.A. Cook, *Nonlinear Dynamical Systems*, Prentice-Hall International (UK) Ltd., Englewood Cliffs, NJ, 1986.
[29] Y.K. Wen, Method of random vibration of hysteretic systems, *Journal of Engineering Mechanics* 102 (1976) 249–263.